

# An Analytical Model for Tailor Welded Blank Forming

**Brad L. Kinsey**

Department of Mechanical Engineering,  
University of New Hampshire,  
Durham, NH 03824-3591

**Jian Cao**

Department of Mechanical Engineering,  
Northwestern University,  
Evanston, IL 60208  
e-mail: jcao@northwestern.edu

*Tailor Welded Blanks (TWBs) offer several notable benefits including decreased part weight, reduced manufacturing costs, increased environmental friendliness, and improved dimensional consistency. In order to take advantage of these benefits, however, designers need to overcome the reduced formability of TWBs and be able to accurately predict unique characteristics related to TWB forming early in the design process. In this paper, an analytical model to predict the weld line movement and forming height for a uniform binder force, TWB forming application is presented. Comparison to numerical simulation results demonstrates the accuracy of this methodology. The analytical model provides designers a valuable tool to determine the location of steps on the die surface to accommodate the weld line movement and the potential forming height for a TWB forming with a uniform binder force. The methodology presented here has the potential to be extended to analyze a non-uniform binder force forming of TWBs. [DOI: 10.1115/1.1537261]*

## Introduction

Automakers are constantly searching for innovative means of reducing vehicle weight and manufacturing costs in order to meet ever-restricting fuel economy standards while remaining economically competitive. A promising opportunity to meet these seemingly conflicting requirements is through the use of Tailor Welded Blanks (TWBs). TWBs are blanks where multiple sheets of material are welded together prior to the forming process. The differences in the material within a TWB can be in the thickness, grade, or coating of the material, e.g., galvanized versus ungalvanized. Figure 1 shows an exploded view of current and/or potential TWB applications for an automotive body-in-white, e.g., front door inner, deck lid, etc. [1]. When creating a TWB, designers are able to tailor, hence the name, the location in the blank where specific material properties are desired. Despite their numerous benefits, forming TWBs is challenging due to a significant reduction of formability associated with this type of blank. First, material property changes in the heat-affected zone of the weld decrease the potential strain in the material prior to tearing failure. The amount of this decrease is dependent on the material type, welding process, and welding parameters used, with reductions in the potential strain prior to tearing failure ranging from 20% to 60% [2–11]. Also, the thinner, weaker material in the TWB may undergo more deformation than the thicker, stronger material in the forming area. This is visually evident in the movement of the weld line towards the thicker material, which can lead to tearing failure in the thinner material. Alternatively, in the binder area, the weld line movement towards the thicker material or the necessity to allow for an initial clearance between the weld line and the step in the binder plate to accommodate thickness differences creates an unconstrained material condition that may lead to wrinkling in the thinner material (see Fig. 2(a) for a schematic of the wrinkling condition). Finally, the weld line may move towards the thinner material in some deep drawing applications, which can lead to tearing failure caused by an over-constrained material condition (see Fig. 2(b) for a schematic of this type of tearing failure).

Extensive research efforts have focused on TWBs with an emphasis on these formability concerns. From the material point of view, studies have been conducted to investigate the material properties of the weld and in heat affected zone [2–4] and the effect of post welding processes, e.g. hot and cold planishing [5].

The decreased formability for popular TWB materials and welding combinations were reported in [6–10]. In the previous work [11], we conducted limit dome height tests of both the base material and TWBs fabricated from 2-mm and 1-mm aluminum 5182-H00 using YAG laser welding with the weld line located in the center of the blank along the major strain direction. From these limit dome height tests, it was determined that the approximate plane strain forming limit was reduced from 22% for the base material to 8% for this TWB combination.

Given the reduced formability of TWBs, modifications to the forming process have been proposed to increase the depth of draw of the formed part. One such method is to increase the material flow-in of the thicker, stronger material to reduce the deformation of the thinner, weaker material through the use of a non-uniform binder force, i.e., a lower binder force is applied to the thicker material than the one applied to the thinner material [12,13]. This technique has shown that if the weld line movement can be prevented, deeper depths of draw can be obtained. Another process modification introduced an additional material constraint within the forming area thus preventing the thinner material from taking a majority of the deformation in the process [14–16]. The additional material constraint method increased the potential depth of draw for a test panel, which included a nonlinear weld line for better material optimization. However, this technique added complexity to the forming process and additional tooling costs.

Though TWBs are currently used in industry, the fundamental understanding to quantify material flow in the process, e.g., weld line movement, is lacking. This consequently results in using a trial and error approach, either numerically or in physical die try-outs, to determine the forming height to achieve a desired strain condition at the weld line and the location of the step in the tooling. In order to utilize TWBs to the fullest potential, a means to determine the forming height and to calculate the weld line movement must be developed. With respect to analytical modeling of TWB applications, little work has been reported. Examples of this research, however, include Shi et al. [17] calculating the limiting thickness and strength difference possible for a TWB application, Cayssials [18] determining the forming limit curve for TWBs, and Doege et al. [4] providing analytical work for the weld properties of TWBs. He et al. [19] used a 2D cross-sectional analysis to determine a non-uniform binder force ratio to improve TWB formability. In their model, the calculations progressed from the edge of the blank to the weld line in order to determine the strain in the 2D cross-section. Good results with respect to determining a non-uniform binder force to prevent weld line movement were obtained and compared with strip and box forming simulations and experiments. The inputs to their model include material

Contributed by the Manufacturing Engineering Division for publication in the JOURNAL OF MANUFACTURING SCIENCE AND ENGINEERING. Manuscript received July 2001; Revised March 2002. Associate Editor: K. A. Stelson.

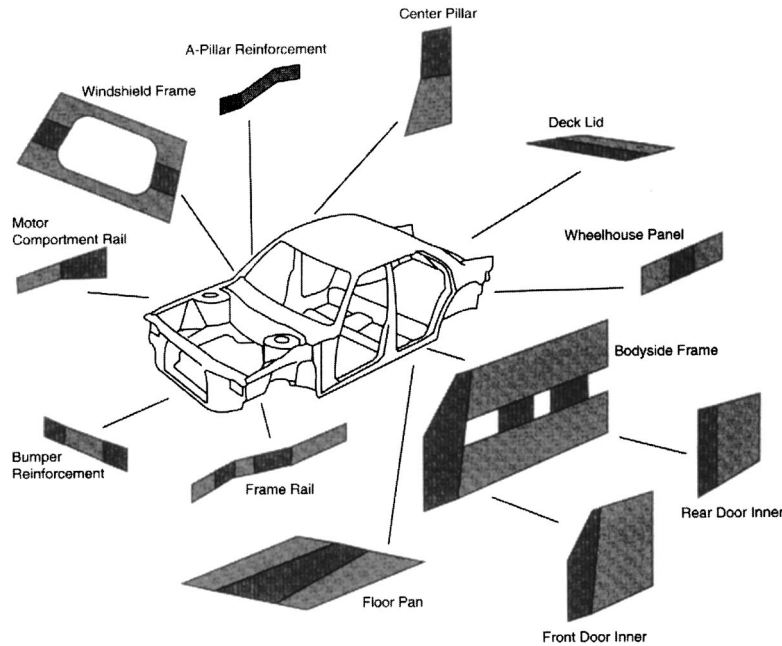


**Fig. 1 Exploded view of current and/or potential automotive TWB applications [1]**

draw-in to the forming area at the edges, the amount of weld line movement, and material flow pattern onto or off the punch face. However, these parameters are not intuitively known prior to numerical simulations or experimental implementation. Using a 2D sectional analysis as was done by He et al. [19] and others [20–22], as oppose to modeling the entire 3D geometry, is a powerful simplification method to analyze the feasibility of sheet metal forming processes.

In this paper, a 2D sectional analysis on various TWB applications is used to analytically determine the weld line movement and forming height for uniform binder force cases. Also, a method to determine the material flow pattern onto and off the punch face is presented. This analytical model would be beneficial to a designer early in the decision making process, prior to costly and time intensive numerical simulations, to determine the potential

depth of draw for a given TWB part and to assure material properties are located where desired in the final part despite weld line movement. Unlike the work presented in the literature, no assumptions regarding material flow in the process are inputted into the model. In order to validate the analytical model, numerical simulations were conducted, and an experimental test panel was formed. Good agreement between the analytical model, the numerical simulations, and test panel forming with respect to weld line movement and forming height demonstrates the effectiveness of this analytical model.

### Methodology of the Analytical Model

The goal of our analytical model is to calculate the weld line movement and forming height for a uniform binder force, TWB application. As was previously mentioned, a 2D sectional analysis greatly simplifies calculations and therefore will be used here. See Fig. 3(a) for a 2D cross-sectional schematic of the tooling geometry and Fig. 3(b) where key locations are identified on the formed TWB. Note that the 1-direction is a local coordinate axis and follows the contour of the 2D cross-section. The location of the cross-section would be taken perpendicular to the weld line and at a position where weld line movement is of interest. For example, the cross-section would be taken where the largest weld line movement, and therefore also largest major principal strain in the thinner material, is expected. Alternatively, several cross-sections could be analyzed to determine material flow over the entire part geometry. The TWB here is represented by two thicknesses with the thicker material on the left side of the 2D cross-section and the thinner material on the right side. Key sections on the 2D cross-section are indicated by capital letters on the thicker side, from A at the weld position to E in the binder area just prior to the die radius, and similarly on the thinner side with lower case letters. All cases presented in this paper assume a flat binder force area with the punch not bottoming out in the lower die (i.e., the parts are formed into air).

In our model, we start at location *a* at the weld line in the 2D cross-section with a known strain level in the 1-direction. Then calculations of force in the 1-direction,  $T_1$ , and strain in the 1-direction,  $\epsilon_1$ , are determined at all locations indicated in Fig. 3(b) proceeding from the weld line towards the blank edge, i.e.,

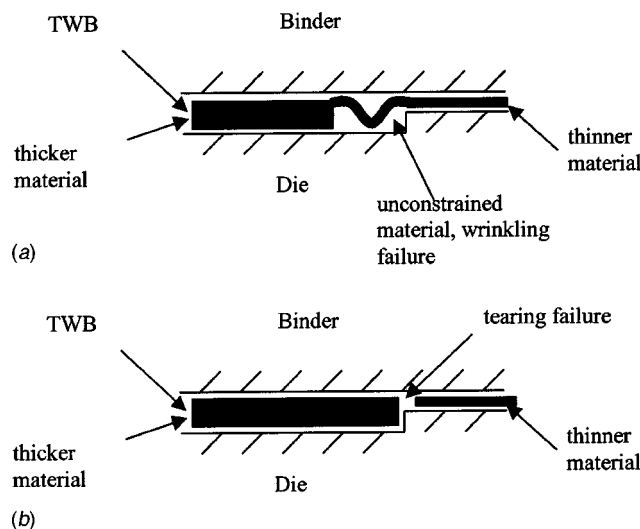


**Fig. 2 Schematic of (a) an unconstrained material condition causing wrinkling failure and (b) an over-constrained material condition causing tearing failure in a TWB application**

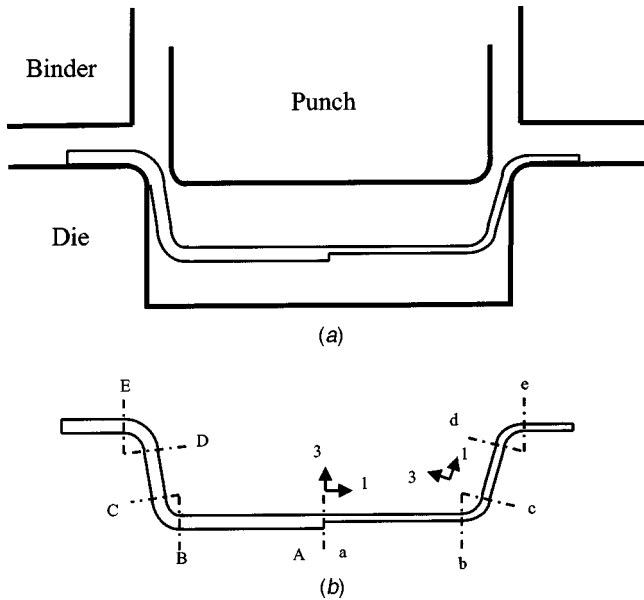


Fig. 3 2D cross-sectional view of (a) TWB and tooling and (b) TWB and key locations identified

from section  $a$  through  $e$  and  $A$  through  $E$ . The analytical model is based on force equilibrium and bending theory.

The methodology for the analytical model is as follows. See also the flowchart in Fig. 4. The value of the strain in the 1-direction at  $a$ , is set to a given value, which could be directly related to a desired outcome such as part stiffness or crashworthiness. To determine the maximum forming height before tearing failure occurs, the strain level can be set to the known plane strain limit, i.e.,  $FLD_0$  value, of the TWB combination. From this strain state, the force per unit width in the 1-direction at section  $a$ , can be calculated.

$$T_{1a} = \sigma_1 t_{thin}^o e^{\varepsilon_{1a}} \quad (1)$$

where  $t_{thin}^o$  is the original thickness of the thinner blank at that location. This relationship is also valid at all locations in the 2D cross-section with the appropriate substitution for variables at the given location. The material is assumed to follow a power hardening law,

$$\bar{\sigma} = K \bar{\varepsilon}^n \quad (2)$$

where  $\bar{\sigma}$  is the equivalent stress and  $\bar{\varepsilon}$  is the equivalent strain.

Due to force equilibrium across the weld line, the same force exists in the material at  $A$ ,  $T_{1A}$ , i.e.,  $T_{1a} = T_{1A}$ . This fact allows the calculation of the strain at  $A$ ,  $\varepsilon_{1A}$ , from force equilibrium. Also, plane strain, no shear stress, incompressibility, and negligible thickness stress,  $\sigma_3 = 0$ , are assumed in our model.

$$\varepsilon_{1A}^n e^{-\varepsilon_{1A}} = \frac{t_{thin}^o}{t_{thick}^o} \varepsilon_{1a}^n e^{-\varepsilon_{1a}} \quad (3)$$

where  $t_{thick}^o$  is the original thickness of the thicker blank at section  $A$ . Force equilibrium can also be applied to all of the locations in the 2D cross-section. In a straight section, a simple force equilibrium is applied, e.g.,  $T_{1a} = T_{1b}$ . This simplification neglects frictional forces in the straight sections of our model, which is a reasonable assumption due to the low value of the frictional forces compared to the forces from material straining. For sections that include a radius, additional force terms for bending,  $\Delta T_{bend}$ , and friction,  $\Delta T_{friction}$ , must be included. The appropriate equations for all of the sections on the thinner side of the TWB are

$$T_{1b} = T_{1a}$$

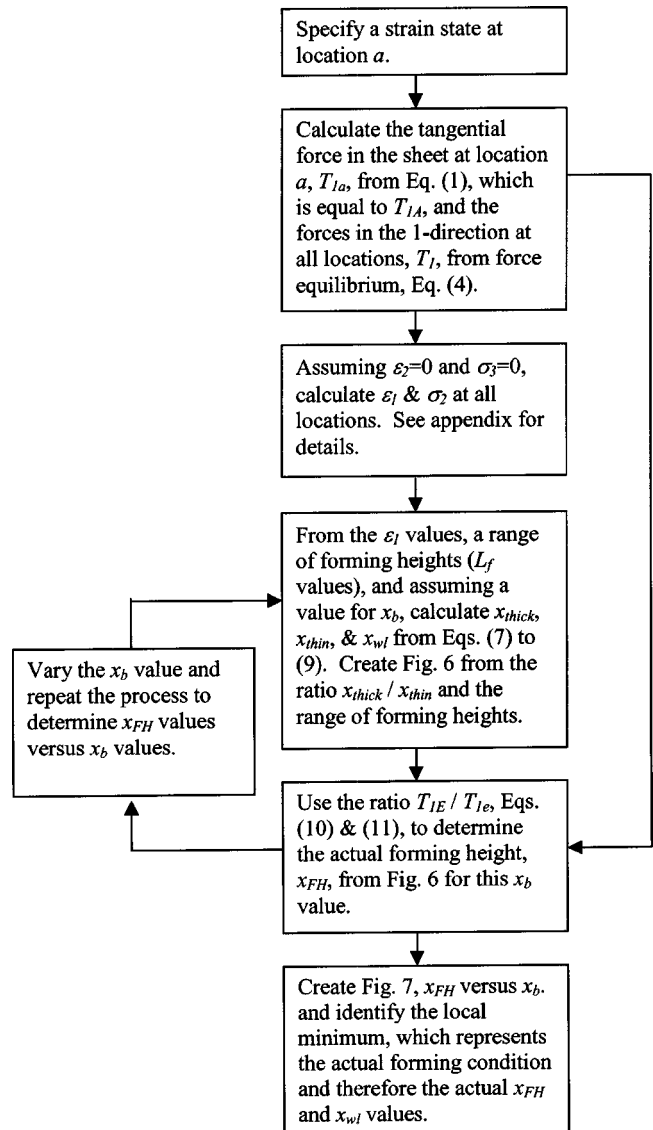


Fig. 4 Flowchart of analytical model methodology

$$T_{1c} = T_{1b} \pm \Delta T_{bend} \pm \Delta T_{friction} \quad (4)$$

$$T_{1d} = T_{1c}$$

$$T_{1e} = T_{1d} - \Delta T_{bend} - \Delta T_{friction}$$

The sign of the  $\Delta T_{bend}$  and  $\Delta T_{friction}$  terms in the  $T_{1c}$  equation depends on whether the material initially at location  $b$  flows onto the punch face (negative) or into the stretch-draw wall area (positive). Similar relationships exist for the thicker side as well. At location  $e$ , the material is assumed to flow into the stretch-draw wall area.

With respect to bending analysis in sheet metal forming, research has investigated using membrane theory in post processing to determine springback [23,24] and shell theory that considers both bending and stretching effects [25–27]. Also, the calculation of tangential strain has been used to determine springback curvature for plane strain bending [19,28]. Here, Swift's model [29] for bending in sheet metal forming is used to calculate  $\Delta T_{bend}$ .

$$\Delta T_{bend} = \frac{2\sigma_y \left(\frac{t}{2}\right)^2}{R} \quad (5)$$

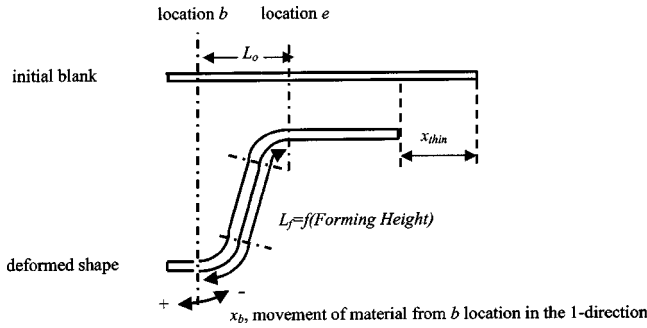


**Fig. 5 Schematic of right side of 2D cross-section showing variables used in material draw-in calculations**

where  $\sigma_y$  is the yield stress of the material,  $t$  is the material thickness, and  $R$  is the bend radius. This model does not account for increased strain in the material due to bending however.

The change in the 1-direction force due to friction,  $\Delta T_{friction}$ , for sections that include a radius is determined from

$$\Delta T_{friction} = T e^{\mu \theta} \quad (6)$$

where  $\mu$  is the friction coefficient and  $\theta$  is the wrap angle around the radius. With these equations for bending and friction, terms for the given part geometry are introduced into the analytical model.

With values calculated for the forces in the 1-direction at all sectional locations, strain values in the 1-direction,  $\epsilon_1$ , and stress values in the 2-direction,  $\sigma_2$ , can be solved from the material constitutive law presented in the appendix. The strain values in the 1-direction can then be used to determine the draw-in on the thicker,  $x_{thick}$ , and thinner,  $x_{thin}$ , sides of the 2D cross-section and the weld line movement,  $x_{wl}$ . Finally, the force values in the 1-direction at  $E$  and  $e$  are used to determine the forming height,  $x_{FH}$ , for the TWB. Further details for calculating  $x_{thick}$ ,  $x_{thin}$ ,  $x_{wl}$ , and  $x_{FH}$  will be presented in the following sections.

### Calculations of Forming Height and Weld Line Movement

In the deep drawing of sheet metal, material movement from under the binder area and the punch face, along with stretching of the material, is essential to produce the wall of the formed part. In order to calculate the forming height,  $x_{FH}$ , at the given strain condition, values for the draw-in of material from under the binder area into the stretch-draw wall are required. For the thinner side of the 2D cross-section, material draw-in,  $x_{thin}$ , can be calculated from

$$x_{thin} = L_f - L_o - (L_f \times e_{be}) \pm x_b \quad (7)$$

where  $L_f$  is the final length of the stretch-draw wall section,  $L_o$  is the length of the material above the stretch-draw wall prior to forming including the punch and die radii,  $e_{be}$  is the engineering strain in the 1-direction from section  $b$  to section  $e$  of the stretch-draw wall, and  $x_b$  is the movement of the material initially at location  $b$  onto the punch face (positive) or into the stretch-draw wall (negative). See Fig. 5 for a graphical representation of these variables on the 2D cross-section. The concept here is that in order to have enough material to create the stretch-draw wall length, even with  $x_b$  material movement considered, material must be draw-in from under the binder, i.e.,  $x_{thin}$ . Note that the draw-in value,  $x_{thin}$ , is a function of the forming height through the  $L_f$  term.

Knowing the value of  $x_b$ , the engineering strain in the 1-direction on the thinner side of the punch face from  $a$  to  $b$ ,  $e_{ab}$ , and the length of this section,  $L_{ab}$ , the weld line movement,  $x_{wl}$ , can be calculated from

$$x_{wl} = (L_{ab} \times e_{ab}) \pm x_b \quad (8)$$

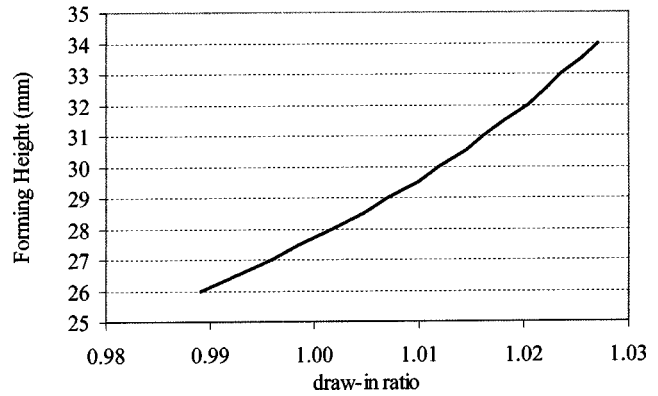


**Fig. 6 Example relationship between material draw-in ratio and forming height**

A similar equation can be now written for material draw-in on the thicker side of the TWB,  $x_{thick}$ . However, for the thicker side, material from the  $x_{wl}$  and the stretching of material on the thicker side of the punch face due to engineering strain,  $e_{AB}$ , also are assumed to flow into the stretch-draw wall on the thicker side. Therefore, these terms are included in the calculation of  $x_{thick}$ .

$$x_{thick} = L_f - L_o - (L_f \times e_{BE}) - (L_{AB} \times e_{AB}) - x_{wl} \quad (9)$$

Again, the material draw-in,  $x_{thick}$ , is dependent on the forming height through the  $L_f$  term.

Equations (7) to (9) provide for a means to calculate  $x_{thin}$  and  $x_{thick}$  for various forming heights (i.e., for various stretch-draw wall length,  $L_f$  values) and for a given value of  $x_b$ . This data can then be plotted to provide a graph of the draw-in ratio,  $x_{thick}/x_{thin}$ , versus forming height for the given  $x_b$  value. A sample plot is provided in Fig. 6. In order to determine the correct forming height for this  $x_b$  value, the ratio of the forces in the 1-direction at  $E$  and  $e$ ,  $T_{1E}/T_{1e}$ , is assumed to be equal to the draw-in ratio, i.e.,

$$\frac{x_{thick}}{x_{thin}} = \frac{T_{1E}}{T_{1e}} \quad (10)$$

The rationale here is that the forces in the 1-direction at  $E$  and  $e$  are the forces that draw material into the stretch-draw wall and therefore their ratio is directly proportional to the ratio of the material draw-in on the thicker and thinner sides. Therefore with a polynomial curve fit of the draw-in ratio versus forming height data, such as that given in Fig. 6, the  $T_{1E}/T_{1e}$  ratio would provide the  $x_{FH}$  for the given  $x_b$  value.

Equation (10) holds if the weld line is located in the center of the blank, i.e., the lengths of the thicker and thinner sides are equal. If the weld line is offset from the center of the blank, this fact needs to be taken into account by adjusting Eq. (10) according to the initial weld line position.

$$\frac{x_{thick}}{x_{thin}} = \frac{T_{1E}}{T_{1e}} \times \left( 1 + \frac{X_{wl}^o}{L_{blank}^o} \right) \quad (11)$$

where  $X_{wl}^o$  is the initial weld line position offset (positive if moved towards the thinner material and negative if moved towards the thicker material) and  $L_{blank}^o$  is the total initial length of the blank.

In the preceding paragraphs, an  $x_b$  value was assumed and the  $x_{FH}$  was determined by relating the draw-in ratio,  $x_{thick}/x_{thin}$ , to the ratio of forces entering the stretch wall area,  $T_{1E}/T_{1e}$ , by either Eq. (10) or (11). In order to determine the actual  $x_b$  value for a given TWB application, the  $x_{FH}$  values for a range of  $x_b$  values must be determined and plotted as shown in Fig. 7. For a reasonable range of  $x_b$  values, a local minimum will exist. From practical forming experiences, it is known that the lowest energy state is the most stable state and therefore, that state corresponds

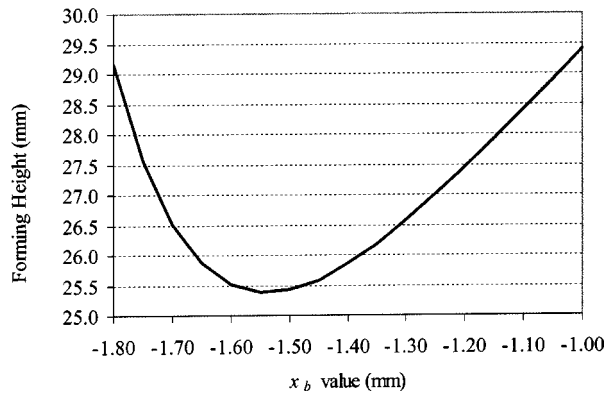


**Fig. 7** Dependency of the calculated forming height,  $x_{FH}$ , on the  $x_b$  value

to a unique and real solution. This concept has been used in solving many engineering problems, for example, in [30,31], however, this is the first time used to calculate the draw-in amount in forming TWBs. In other words, there exists a lowest energy state that will be created for a set of process parameters thus producing a unique forming height and draw-in condition. Therefore, it can be concluded that the minimum forming height for various  $x_b$  values shown in Fig. 7 corresponds to that unique forming height. Consequently, this  $x_b$  represents the actual movement of the material off the punch face into the stretch-draw wall. A graph similar to Fig. 6 can be created for the actual  $x_b$  value and  $x_{FH}$  and  $x_{wl}$  can be determined as described above. These values represent the actual  $x_{FH}$  and  $x_{wl}$  for the given TWB application.

### Numerical Simulations

In order to verify our analytical model, numerical simulations were conducted on the commercially available FEM software ABAQUS/Standard. Figures 8(a) and (b) show the two geometries that were used in these simulations, Geometries I and II, respectively. Plane strain, four node, reduced integration elements, ABAQUS type CPE4R, were used to simulate the plane strain problem. The number of layers through the thickness varied based on the material thickness used with the element density being 0.25-mm/element for Geometry I and 0.20-mm/element for Geometry II. The exact number of layers through the thickness can be determined from this element density and the specific thickness value given in Table 1 for each individual case. Other simulation parameters included a Coulomb friction coefficient of 0.15, material properties used in the power hardening law,  $K = 570$  MPa and  $n = 0.3$ , and a uniform binder force of 200-kN for Geometry I and 120-kN for Geometry II. The FEM models were developed to reach a draw depth of 30-mm when the given strain state was reached. For the case of Geometry I, the strain magnitude at location  $a$  was set to be 8% since this strain state has been shown to produce tearing failure for an AA5182 2-mm and 1-mm TWB [11,15]. Therefore, the forming height with this strain level would be the failure height for this geometry. For Geometry II, the strain state was set to an arbitrary value of 4.7%, which was determined from a numerical simulation of the given geometry and parameters. This demonstrates the ability to enter various desired strain levels at location  $a$  into the model and obtain accurate results.

### Comparison of Analytical Model and Numerical Simulations

In post processing the numerical simulation results, forces and strains in the 1-direction,  $T_1$  and  $\epsilon_1$ , were extracted to compare with values obtained from the analytical model. Figure 9 shows a plot of  $T_1$  obtained from both the analytical model and the numerical simulation of Geometry I with the initial weld position in

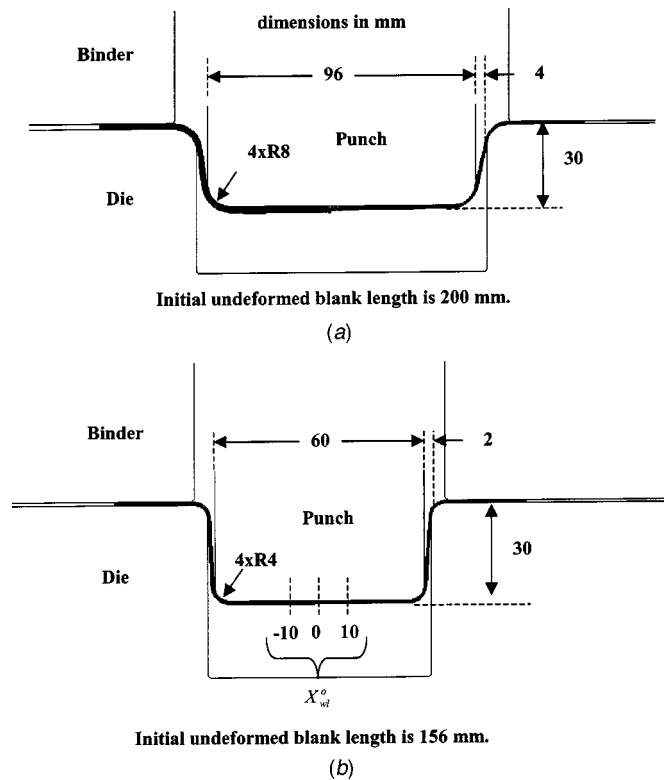


**Fig. 8** 2D cross-sectional geometry for (a) Geometry I and (b) Geometry II, which also indicates initial weld line positions

the center of the blank normalized by the force in the 1-direction at the weld line, i.e., at sections  $A$  and  $a$ . Excellent agreement exists at all sectional locations. Figure 10 shows a plot of  $\epsilon_1$  for both the analytical model and the numerical simulations normalized by the strain at  $A$  and  $a$  for the thicker and thinner sides respectively. In this plot, agreement is reasonable for all sectional locations except for  $D$  and  $d$ , i.e., where the die radii lead into the stretch-draw walls. This is due to the simplified bending model used in our analysis, Eq. (5). While this discrepancy seems large on the thicker side at  $D$ , since the strain value is small at this location, only 0.1% in the analytical model, the effect on material draw-in values is negligible. The agreement between the analytical model and numerical simulation in Figs. 9 and 10 demonstrates the accuracy of the analytical model calculations, which will be further examined through the geometry presented in the following section.

Table 1 compares the results of  $x_{wl}$  and  $x_{FH}$  values for eleven cases with various initial weld line positions and TWB combinations, i.e., the thickness difference in the TWB application. As was stated previously, the negative numbers for the initial weld line positions indicate offsetting the weld line from the center position into the thicker material and positive numbers indicate offsetting the weld line into the thinner material. Figure 8(b) also shows the initial weld line positions for Geometry II for clarity. For all the cases, the maximum discrepancies with respect to weld line movement were 1.42-mm and 0.53-mm and with respect to forming height were 5.00-mm and 6.44-mm, for Geometry I and Geometry II respectively. The case of Geometry II with the weld line offset 10-mm towards the thinner material demonstrates that as the location of the weld line approaches the punch radius on the thinner side, the prediction of the forming height is over predicted, while in all of the other cases, the forming height was under predicted. However, good agreement exists between the numerical simulations and the analytical model for all of the cases.

**Table 1 Results comparing analytical model calculations to 2D numerical simulations**

Geometry	TWB combination (thick/thin)	$X_{wl}^o$ (mm)	$x_{wl}$ 2D sim. (mm)	$x_{wl}$ anal. (mm)	$x_{FH}$ 2D sim. (mm)	$x_{FH}$ anal. (mm)
I	2.0/1.0 mm	-24	5.53	4.18	30	25.00
		-16	4.92	3.61		25.03
		-8	4.47	3.05		25.12
		0	3.74	2.53		25.36
		8	2.99	1.92		25.63
		16	2.43	1.35		26.26
I	1.5/1.0 mm	0	2.38	2.23	30	24.76
		-10	2.23	2.09		23.56
II	1.0/0.6 mm	0	1.66	1.26	30	23.84
		10	1.06	0.53		36.38
		0	1.08	0.75		24.75

**Application of Analytical Model to Test Panel**

As an example of the application of the analytical model to a TWB part, consider the test panel punch and blank geometry shown in Fig. 11, which emulates a door inner. This geometry was used in previous research projects in our laboratory [15,16]. The

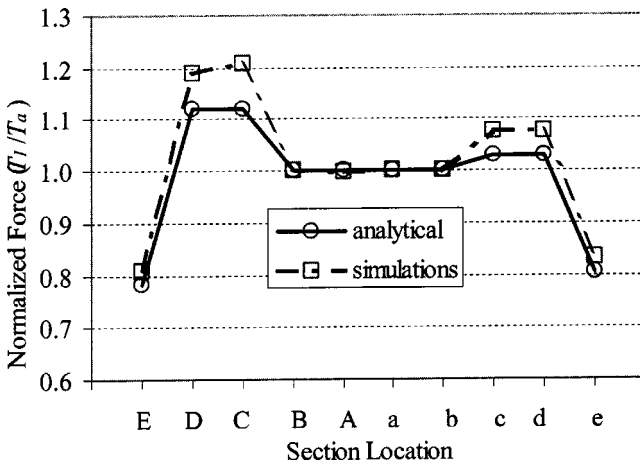


**Fig. 9 Comparison of normalized force in the 1-direction obtained from the analytical model and numerical simulation. Case shown is Geometry I with the initial weld line position in the center.**

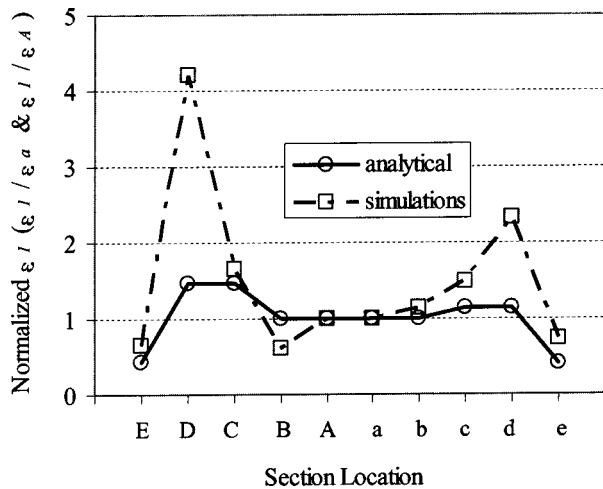


**Fig. 10 Comparison of normalized strain in the 1-direction obtained from the analytical model and numerical simulation. Case shown is Geometry I with the initial weld line position in the center.**

line shown on the test panel indicates where the 2D cross-section was chosen for the analytical model on this part geometry. This location was selected because the maximum weld line movement occurred where the slanted and vertical weld lines intersect for this particular application. Figure 12 shows the 2D cross-sections used in the ABAQUS 2D numerical simulation. A 220-kN binder force was applied in the simulation. In full test panel experimental implementation and a 3D numerical simulation using LSDYNA software (see [16] for details), failure in the test panel was shown to occur at approximately 77.3-mm of draw depth with 11.63-mm of weld line movement and a strain condition of 8% major principal strain and -5% minor principal strain [15,16]. Table 2 provides a comparison between the full 3D numerical simulation, the 2D numerical simulation, and the analytical model. The failure height and weld line movement obtained from the 2D numerical simulation agrees well with those obtained from the analytical model, failure height of 80-mm and 69.3-mm and weld line movement of 19.3-mm and 17.4-mm for the 2D simulation and analytical model respectively. For the 3D numerical simulations, a reasonable agreement was obtained, failure height of 77.3-mm and 69.3-mm and weld line movement of 11.6-mm and 17.4-mm for the 3D simulation and analytical model respectively. These discrepancies in the analytical model compared to the 3D simulation can be attributed to the fact that the strain condition in the full 3D numerical simulation and experiments is not exactly a plane strain condition, approximately -5% deep drawing condition, while the analytical model assumed a plane strain condition. Nevertheless, this example demonstrates how the analytical model could have been used effectively prior to numerical simulations and experimental implementation to estimate the potential forming height and weld line movement for this TWB application.

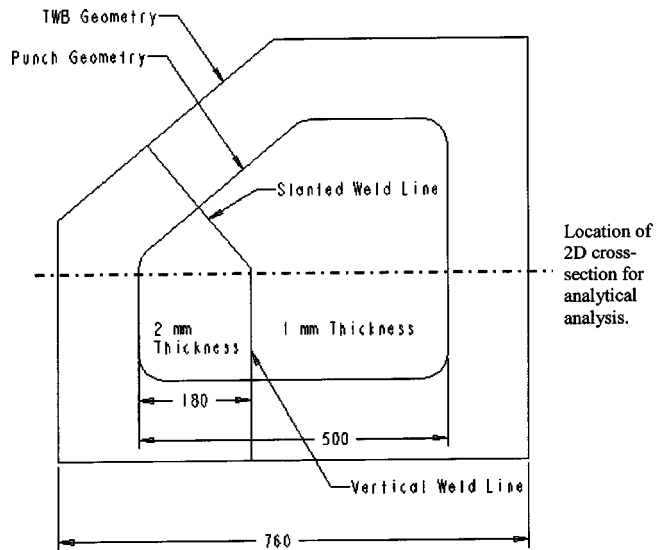


**Fig. 11 Location of 2D cross-section on test panel geometry**

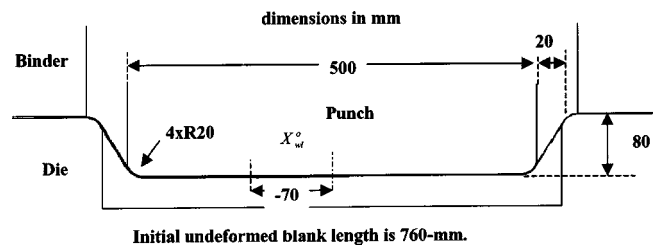


**Fig. 12 2D cross-sectional geometry for test panel geometry, which also indicates initial weld line position**

**Table 2 Results comparing analytical model calculations to 2D and 3D numerical simulations for the test panel geometry**

Geometry	TWB combination (thick/thin)	$X_{wl}^o$ (mm)	$x_{wl}$	$x_{wl}$	$x_{wl}$ anal. (mm)	$x_{FH}$	$x_{FH}$	$x_{FH}$ anal. (mm)
			3D sim. (mm)	2D sim. (mm)		3D sim. (mm)	2D sim. (mm)	
Test panel	2.0/1.0	-70	11.6	19.3	17.4	77.3	80	69.3

## Conclusions and Discussion

Tailor Welded Blanks offer numerous advantages over the conventional method to fabricate sheet metal parts, e.g., body-in-white components in the automotive industry. However, decreased formability caused by weld line movement and changes in the material properties in the heat-affected zone of the weld limit their utilization. In order to aid in the design process, an analytical model was developed and presented here to assist the designer in determining the amount of weld line movement and the forming height for a given TWB geometry. Knowledge of these parameters is critical early in the design process so the designer is able to locate the material properties in the formed part where desired and assure the necessary depth of draw is obtainable. A 2D sectional analysis was utilized, and values for material draw-in from under the binder ring were determined in order to obtain the desired parameters. Good agreement between the analytical model and numerical simulations with respect to both weld line movement and forming height verifies the effectiveness of the methodology.

While this analytical model was shown to provide good results compared to numerical simulations, there are several aspects of the model that should be noted. First, plane strain and negligible thickness stress assumptions were used to solve the non-linear equations, but these assumptions limit the effectiveness of the model for general cases. In particular, the plane strain assumption could be eliminated to allow for bi-axial straining to be possible, either deep drawing with a negative minor strain or stretch forming with a positive minor strain, at locations on the 2D cross-section. This would allow the model to be used in a more general fashion. Also, the simple bending model used here could be replaced with a model that includes additional stretching of the material due to bending. This would allow the analytical model to follow the numerical simulations more accurately at locations  $D$  and  $d$  where additional stretching due to bending occurs (see Fig. 10). In addition, some fundamental mechanics may exist between Eqs. (10) and (11), which relate the draw-in ratio to the ratio of forces at  $E$  and  $e$  and the initial weld line position. Future work will further investigate this relationship and explore added cases to verify the validity of these equations. Finally, the material model could be replaced by an alternative constitutive model depending on the material being formed. Despite these noted details, the analytical model presented in this paper provides a powerful tool for designers to analyze TWB applications prior to costly and time-consuming numerical simulations and part implementation thus providing a considerable benefit.

## Acknowledgments

This research was funded by NSF Grant DMI-9703249 and the Engineering Research Program of the Office of Basic Energy Sciences at the Department of Energy.

## Nomenclature

- $\epsilon_{1i}$  = true strain in the 1-direction at location  $i$
- $F, G, H$  = parameters reflecting the material's anisotropy
- $L_{blank}^o$  = initial length of TWB
- $L_f$  = final length of the stretch-draw wall
- $L_{ij}$  = initial length of a section from location  $i$  to  $j$

- $L_o$  = initial length of material above the stretch-draw wall prior to forming
- $R$  = bend radius of punch and/or die
- $T_{1i}$  = force in the 1-direction at location  $i$
- $X_{wl}^o$  = offset of weld line from the center of the TWB
- $e_{ij}$  = engineering strain in the stretch-draw wall from location  $i$  to  $j$
- $n$  = strain hardening exponent
- $t$  = sheet thickness
- $t_{thin}^o$  = original thickness of the thinner blank
- $t_{thick}^o$  = original thickness of the thicker blank
- $x_b$  = movement of the material initially at location  $b$  onto the punch face or into the stretch-draw wall
- $x_{FH}$  = forming height at given strain state for location  $a$
- $x_{thick}$  = material draw-in from the binder area on the thicker blank side
- $x_{thin}$  = material draw-in from the binder area on the thinner blank side
- $x_{wl}$  = weld line movement
- $\epsilon_i$  = true strain in the 1-direction at location  $i$
- $\bar{\epsilon}$  = equivalent strain
- $d\lambda$  = plastic potential
- $\Delta T_{bend}$  = additional force term due to bending
- $\Delta T_{friction}$  = additional force term due to friction
- $\mu$  = friction coefficient
- $\bar{\sigma}$  = equivalent stress
- $\sigma_i$  = true stress in the  $i$ -direction
- $\sigma_y$  = true stress at yielding
- $\theta$  = wrap angle around punch and/or die radius

## Appendix: Material Constitutive Laws

In order to calculate the  $x_{wl}$  and  $x_{FH}$ , the stress and strain values at each location in the 2D cross-section must be calculated. The material is assumed to follow Hill's 1948 yield criterion [32] and the associated flow rule,

$$F(\sigma_2 - \sigma_3)^2 + G(\sigma_3 - \sigma_1)^2 + H(\sigma_1 - \sigma_2)^2 = 2f(\sigma_{ij}) = 2\bar{\sigma}^2 \quad (A1)$$

where  $F$ ,  $G$ , and  $H$  are the parameters reflecting the material's anisotropy and  $\sigma_i$  are the principal stresses. To relate strain to the stress in plastic deformation, the flow rule is utilized

$$\epsilon_{ij} = d\lambda \frac{\partial f(\sigma_{ij})}{\partial \sigma_{ij}} \quad (A2)$$

where  $d\lambda$  is the plastic potential. Differentiating Eq. (A1) with respect to the three principal stresses and substituted into the flow rule, the following equations are obtained

$$\begin{aligned} d\epsilon_1 &= d\lambda [H(\sigma_1 - \sigma_2) + G(\sigma_1 - \sigma_3)] \\ d\epsilon_2 &= d\lambda [F(\sigma_2 - \sigma_3) + H(\sigma_2 - \sigma_1)] \\ d\epsilon_3 &= d\lambda [G(\sigma_3 - \sigma_1) + F(\sigma_3 - \sigma_2)] \end{aligned} \quad (A3)$$

The equivalent strain,  $\bar{\epsilon}$ , is defined by the work conjugate equation

$$dw = \sigma_{ij} d\epsilon_{ij} = 2f(\sigma_{ij}) = 2\bar{\sigma}^2 = \bar{\sigma} \bar{\epsilon} \quad (A4)$$

This equation can then be solved for  $d\lambda$  to give

$$d\lambda = \frac{\bar{\varepsilon}}{2\bar{\sigma}} \quad (A5)$$

Assuming a linear strain path and manipulating Eqs. (A3) and (A5), an equation for the equivalent strain is expressed as

$$\bar{\varepsilon} = \sqrt{2} \left[ F \left( \frac{G\varepsilon_2 - H\varepsilon_3}{FG + GH + HF} \right)^2 + G \left( \frac{H\varepsilon_3 - F\varepsilon_1}{FG + GH + HF} \right)^2 + H \left( \frac{F\varepsilon_1 - G\varepsilon_2}{FG + GH + HF} \right)^2 \right]^{1/2} \quad (A6)$$

For the plane strain case, Eq. (A6) reduces to

$$\bar{\varepsilon} = \sqrt{2} \left[ \frac{FH^2 + G(H+F)^2 + HF^2}{(FG + GH + HF)^2} \right]^{1/2} \varepsilon_1 \quad (A7)$$

Once  $\bar{\varepsilon}$  is known,  $\bar{\sigma}$  can be obtained from the material power law relationship, Eq. (2).

Substituting Eq. (A5) into Eq. (A3) and evoking the plane strain and negligible thickness stress assumptions, we have

$$\begin{aligned} \varepsilon_1 &= \frac{\bar{\varepsilon}}{2\bar{\sigma}} [H(\sigma_1 - \sigma_2) + G\sigma_1] \\ \varepsilon_2 &= \frac{\bar{\varepsilon}}{2\bar{\sigma}} [F\sigma_2 + H(\sigma_2 - \sigma_1)] \\ \varepsilon_3 &= \frac{\bar{\varepsilon}}{2\bar{\sigma}} [-G\sigma_1 - F\sigma_2] \end{aligned} \quad (A8)$$

Equations (1), (2), and (A8) represent non-linear functions. Therefore, Newton's method to solve simultaneous non-linear equations was utilized. From these equations and also Eq. (A7), all of the  $\varepsilon$  and  $\sigma$  values at each location in the 2D cross-section can be determined. For instance, at location  $a$ , the strain state is given and the stress state can be calculated,  $\sigma_{1a}$  and  $\sigma_{2a}$ . Also, with the force in 1-direction known at each location from Eq. (4) and the relationship between  $T_1$  and  $\sigma_1$  being governed by Eq. (1),  $\varepsilon_1$  and  $\sigma_2$  can be calculated at each location,  $b$  through  $e$ , for both the thinner and thicker sides of the 2D cross-section.

## References

- [1] Auto/Steel Partnership, 1995, "Tailor Welded Blank Design and Manufacturing Manual," Technical Report.
- [2] Eisenmenger, M., Bhatt, K. K., and Shi, M. F., 1995, "Influence of Laser Welding Parameters on Formability and Robustness of Blank Manufacturing: An Application to a Body Side Frame," SAE Technical Paper Series, Paper No. 950922, pp. 171–182.
- [3] Bhatt, K. K., Eisenmenger, M., and Shi, M. F., 1995, "Formability of Mash Seam Welded Blanks: Effects of Welding Set-Up Conditions," SAE Technical Paper Series, Paper No. 950923, pp. 183–189.
- [4] Doege, E., Dohrmann, H., and Koters, R., 1996, "Simulation and Optimization of the Forming Process of Tailored Blanks," *Proceedings of Numisheet '96*, pp. 199–204.
- [5] Lee, A. P., Feltham, E., and Van Deventer, J., 1996, "Tailor Welded Blank Technology for Automotive Applications," *Sheet Metal Stamping for Automotive Applications*, SAE Technical Paper Series, Paper No. 960817, pp. 91–102.
- [6] Kridli, G. T., Friedman, P. A., and Sherman, A. M., 2000, "Formability of Aluminum Tailor-Welded Blanks," SAE Paper No. 2000-01-0772.
- [7] Venkat, B. S., Albright, C. E., Ramasamy, S., and Hurley, J. P., 1997, "CO<sub>2</sub> Laser Beam Welding of Aluminum 5754-O and 6111-T4 Alloys," *Weld. J. (Miami)*, **76**(7), July, pp. 275–82s.
- [8] Stasik, M. C., and Wagoner, R. H., 1996, "Forming of Tailor Welded Aluminum Blanks," *Aluminum and Magnesium for Automotive Applications*, The Minerals, Metals & Materials Society, pp. 69–83.
- [9] Davies, R. W., Smith, M. T., Oliver, H. E., Khaleel, H., Pitman, S. G., 2000, "Weld Metal Ductility in Aluminum Tailor Welded Blanks," *Metall. Mater. Trans. A*, **31**(11), pp. 2755–2763.
- [10] Davies, R. W., Grant, G. J., Oliver, H. E., Khaleel, H., Smith, M. T., 2001, "Forming-limit Diagrams of Aluminum Tailor-Welded Blank Weld Material," *Metall. Mater. Trans. A*, **32**(2), pp. 275–283.
- [11] Viswanathan, V., Kinsey, B., and Cao, J., 2001, "Forming of Aluminum Tailor Welded Blanks," SAE Paper No. 2000-01-0822.
- [12] Ahmetoglu, M. A., Brouwers, D., Shulkin, L., Taupin, L., Kinzel, G. L., and Altan, T., 1995, "Deep Drawing of Round Cups from Tailor-welded Blanks," SAE Trans. **53**, pp. 684–694.
- [13] Siegert, K., and Knabe, E., 1995, "Fundamental Research and Draw Die Concepts for Deep Drawing of Tailored Blanks," SAE Trans., **104**, pp. 866–876.
- [14] Cao, J., and Kinsey, B., 1999, "Adaptive Method and Apparatus for Forming Tailor Welded Blanks," U.S. Patent No. 5,941,110.
- [15] Kinsey, B., and Cao, J., 2001, "Enhancement of Sheet Metal Formability Via Local Adaptive Controllers," *Transactions of NAMRI of SME*, Vol. XXIX, pp. 81–88.
- [16] Kinsey, B., and Cao, J., 2001, "Numerical Simulations and Experimental Implementation of Tailor Welded Blank Forming," *Second Global Symposium on Innovations in Materials Processing & Manufacturing: Sheet Materials*, 2001 TMS Annual Meeting.
- [17] Shi, M. F., Pickett, K. M., and Bhatt, K. K., 1993, "Formability Issues in the Application of Tailor Welded Blank Sheets," SAE Trans., Paper No. 930278, **102**(5), pp. 27–35.
- [18] Cayssials, F., 2000, "An Industrial Application of Specific Forming Limit Curves for Tailor Welded Blanks," *Proceedings of the 2000 International Deep Drawing Research Group*, Ann Arbor, MI, June, pp. 17–22.
- [19] He, S., Wu, X., and Hu, S. J., 2001, "Formability Enhancement for Tailor-Welded Blanks Using Blank Holding Force Control," *2001 ASME International Congress of Mechanical Engineering Congress & Exposition*.
- [20] Saran, M. J., Keum, Y. T., and Wagoner, R. H., 1991, "Section Analysis with Irregular Tools and Arbitrary Draw-in Conditions for Numerical Simulation of Sheet Forming," *Int. J. Mech. Sci.*, **33**(11), pp. 893–909.
- [21] Brooks, A., Jhita, R., and Ni, C. M., 1991, "Applications of a Two-Dimensional Metal Forming Analysis Tool to Production Stamping Problems," SAE Trans., Paper No. 910775, **100**(5), pp. 751–758.
- [22] Hong, Y., Brad, Kinsey, and Jian, Cao, 2000, "Rapid Design of Corner Restraining Force in Deep Drawn Rectangular Parts," *Int. J. Mach. Tools Manuf.*, **40**(1), pp. 113–131.
- [23] Wenner, M. L., 1983, "On Work Hardening and Springback in Plane Strain Draw Forming," *Journal of Applied Metal Working*, **2**(4), p. 277.
- [24] Pourboghra, F., and Chandorkar, K., 1992, "Springback Calculation for Plane Strain Sheet Forming Using Finite Element Membrane Solution," *Numerical Methods for Simulation of Industrial Metal Forming Processes*, CED-Vol. 5, AMD- Vol. 156, p. 85.
- [25] Wang, N. M., and Tang, S. C., 1988, "Analysis of Bending Effects in Sheet Forming Operations," *Int. J. Numer. Methods Eng.*, **25**, p. 253.
- [26] Wang, N. M., and Wenner, M. L., 1978, "Elastic-viscoplastic Analysis of Simple Stretch Forming Problems," *Mechanics of Sheet Metal Forming*, Koistinen, D. P., and Wang, N. M., eds., Plenum Press, New York, p. 367.
- [27] Wood, R. D., Mattiasson, K., Honnor, M. E., and Zienkiewicz, O. C., 1985, "Viscous Flow and Solid Mechanics Approaches to the Analysis of Thin Sheet Forming," *Computer Modeling of Sheet Metal Forming Processes*, Wang, N. M., and Tang, S. C., eds., AIME.
- [28] Zhang, Z. T., and Hu, S. J., 1997, "Mathematical Modeling in Plane Strain Bending," SAE Trans., Paper No. 970439, **106**(5), pp. 63–76.
- [29] Swift, H. W., 1948, "Plastic Bending under Tension," *Engineering*, **166**, pp. 333–359.
- [30] Hutchinson, J. W., and Neale, K. W., 1985, "Wrinkling of Curved Thin Sheet Metal," *Plastic Instability*, Presses Ponts et Chaussées, Paris, pp. 71–78.
- [31] Yu, T. X., and Johnson, W., 1982, "The Buckling of Annular Plates in Relation to the Deep-Drawing Process," *Int. J. Mech. Sci.*, **24**, pp. 175–188.
- [32] Hill, R., 1950, *The Mathematical Theory of Plasticity*, Oxford University Press, London.